JNeurosci
THE JOURNAL OF NEUROSCIENCE

Research Articles: Cellular/Molecular

Loss of protein arginine methyltransferase 8 alters synapse composition and function, resulting in behavioral defects.

Jay Penney[1,2], Jinsoo Seo[1,2], Oleg Kritskiy[1,2], Sara Elmsaouri[1,2], Fan Gao[1,2], Ping-Chieh Pao[1,2], Susan C. Su[1,2] and Li-Huei Tsai[1,2]

[1]*The Picower Institute for Learning and Memory*
[2]*Department of Brain and Cognitive Sciences, Massachusetts Institute of Technology, Cambridge, MA, USA, 20139*

DOI: 10.1523/JNEUROSCI.0591-17.2017

Received: 2 March 2017

Revised: 6 July 2017

Accepted: 25 July 2017

Published: 3 August 2017

Author contributions: J.P. and L.-H.T. designed research; J.P., J.S., O.K., S.E., P.-C.P., and S.C.S. performed research; J.P., J.S., O.K., and F.G. analyzed data; J.P. and L.-H.T. wrote the paper.

Conflict of Interest: The authors declare no competing financial interests.

This work was partially funded by the National Institutes of Health (grant 2-R37-NS051874-21 to LHT), the Belfer Neurodegeneration Consortium and a Human Frontier Science Program Long Term Fellowship to JP. We thank A. Waston and N. Dedic for insightful comments, and E. McNamara for animal maintenance.

Corresponding author: Li-Huei Tsai, The Picower Institute for Learning and Memory, Department of Brain and Cognitive Sciences, Massachusetts Institute of Technology, 77 Massachusetts Ave., Cambridge, MA, USA, 20139. lhtsai@mit.edu

Cite as: J. Neurosci ; 10.1523/JNEUROSCI.0591-17.2017

Title: **Loss of protein arginine methyltransferase 8 alters synapse composition and function, resulting in behavioral defects.**

Abbreviated title: PRMT8 regulates hippocampal function and plasticity

Author names and affiliation: Jay Penney[1,2], Jinsoo Seo[1,2], Oleg Kritskiy[1,2], Sara Elmsaouri[1,2], Fan Gao[1,2], Ping-Chieh Pao[1,2], Susan C. Su[1,2], Li-Huei Tsai[1,2].

[1]The Picower Institute for Learning and Memory,

[2]Department of Brain and Cognitive Sciences, Massachusetts Institute of Technology, Cambridge, MA, USA, 20139

Corresponding author: Li-Huei Tsai

The Picower Institute for Learning and Memory

Department of Brain and Cognitive Sciences, Massachusetts Institute of Technology, 77 Massachusetts Ave., Cambridge, MA, USA, 20139. lhtsai@mit.edu

Number of pages: 37

Number of figures: 7

Number of words, Abstract: 138, Introduction: 431, Discussion: 1500

Conflict of interest: The authors declare no competing financial interests.

Acknowledgements: This work was partially funded by the National Institutes of Health (grant 2-R37-NS051874-21 to LHT), the Belfer Neurodegeneration Consortium and a Human Frontier Science Program Long Term Fellowship to JP. We thank A. Waston and N. Dedic for insightful comments, and E. McNamara for animal maintenance.

Abstract

Diverse molecular mechanisms regulate synaptic composition and function in the mammalian nervous system. The multifunctional protein arginine methyltransferase 8 (PRMT8) possesses both methyltransferase and phospholipase activities. Here we examine the role of this neuron-specific protein in hippocampal plasticity and cognitive function. PRMT8 protein localizes to synaptic sites and conditional whole brain *Prmt8* deletion results in altered levels of multiple synaptic proteins in the hippocampus, using both male and female mice. Interestingly these altered protein levels are due to post-transcriptional mechanisms as the corresponding mRNA levels are unaffected. Strikingly, electrophysiological recordings from hippocampal slices of mice lacking PRMT8 reveal multiple defects in excitatory synaptic function and plasticity. Furthermore, behavioral analyses show that PRMT8 conditional knockout mice exhibit impaired hippocampal-dependent fear learning. Together these findings establish PRMT8 as an important component of the molecular machinery required for hippocampal neuronal function.

Significance Statement

Numerous molecular processes are critically required for normal brain function. Here we use mice lacking protein arginine methyltransferase 8 (PRMT8) in the brain to examine how loss of this protein affects the structure and function of neurons in the hippocampus. We find that PRMT8 localizes to the sites of communication between neurons. Hippocampal neurons from mice lacking PRMT8

have no detectable structural differences compared to controls; however, multiple aspects of their function are altered. Consistently we find that mice lacking PRMT8 also exhibit reduced hippocampus-dependent memory. Together our findings establish important roles for PRMT8 in regulating neuron function and cognition in the mammalian brain.

Introduction

A myriad of molecular mechanisms regulate synaptic plasticity and cognitive processes in the mammalian brain. The regulation of gene expression, mRNA trafficking to synaptic sites and numerous post-translational mechanisms including protein trafficking, phosphorylation, ubiquitination and acetylation are all critical to neuronal function (Kandel, 2001). The protein arginine methyltransferase (PRMT) family of enzymes regulates numerous cellular processes and pathways; however the roles of these proteins in brain function have only begun to be explored (Bedford and Clarke, 2009).

PRMT8 is unique among the PRMT proteins in that it is expressed specifically in the nervous system (Lee et al., 2005; Kousaka et al., 2009). Furthermore, PRMT8 is a multifunctional protein, exhibiting both arginine methyltransferase and phospholipase D activities (Lee et al., 2005; Kim et al., 2015). Phospholipase D enzymes play important roles in nervous system development and function, while the identification of many arginine-methylated synaptic proteins suggests that this modification may also be an important regulator of synapse biology (Klein, 2005;

Burkhardt et al., 2014; Guo et al., 2014). PRMTs, including PRMT8, have been ascribed nuclear roles in regulating gene expression; however PRMT8 protein can be myristoylated and membrane-targeted, suggesting it could localize to synaptic sites as well (Lee et al., 2005; Bedford and Clarke, 2009; Simandi et al., 2015; Lee et al., 2017).

The zebrafish PRMT8 ortholog was found to be important for nervous system development, while mouse studies suggest roles for PRMT8 in cerebellar granule neurons, as well as in GABAergic interneurons of the visual cortex (Kim et al., 2015; Lee et al., 2017). Kim et al. (2015) showed that conditional *Prmt8* deletion inhibited the arborization of granule cells and reduced acetylcholine levels in the cerebellum. More recently, Lee et al. (2017) found that *Prmt8* mutation affected perineuronal net formation in the visual cortex, as well as visual acuity of mutant mice. Thus far the potential effects of PRMT8 on synaptic function and cognitive processes have not been explored.

Here, we examine the roles of PRMT8 in hippocampal neuronal morphology, composition and function. We find that PRMT8 protein localizes to pre- and post-synaptic sites, but that loss of PRMT8 does not affect synapse density, or dendritic spine density or morphology. PRMT8 conditional deletion with *Nestin-cre* does, however, alter levels of a number of synaptic proteins and affect multiple measures of synaptic function and plasticity. Further, while PRMT8 mutation does not significantly alter locomotor or anxiety-related behaviors, context-dependent fear

learning is impaired in *Prmt8* conditional knockout mice. Together these findings establish novel roles for PRMT8 in regulating excitatory synapse composition and function as well as cognitive processes, in the mammalian nervous system.

Materials and Methods

Mice: All experiments were performed according to the Guide for the Care and Use of Laboratory Animals and were approved by the National Institutes of Health and the Committee on Animal Care at the Massachusetts Institute of Technology. *Prmt8*$^{tm1a(EUCOMM)Wtsi}$ (Skarnes et al., 2011) embryos were obtained from the European Mutant Mouse Consortium. Following re-derivation the mice were crossed to FLP recombinase expressing mice (Vooijs et al., 1998) to generate mice with the *Prmt8* 5th exon flanked by loxP sites. Following intercrosses to generate homozygous *Prmt8* floxed mice they were bred to *Nestin-cre* expressing mice (Tronche et al., 1999) to conditionally delete *Prmt8* exon 5. *Prmt8* floxed/*Prmt8* floxed mice served as controls, while experimental mice were *Prmt8* floxed/*Prmt8* floxed; *Nestin-cre*/+ (referred to as *Prmt8* cKO). 10-14 week old mice were used for all experiments except for mIPSC and GluN2A-mediated recordings. Mice for these latter experiments were 16-18 weeks old. Male mice were used for immunostaining, Golgi staining, electrophysiology and behavior experiments. Both male and female mice were used for qPCR and biochemistry experiments.

Primary neuronal culture: Primary forebrain neurons were cultured from E16.5 Swiss Webster embryos and analyzed at DIV17. Briefly, forebrains were removed,

115 digested with Papain and plated on poly-D-lysine (PDL; Sigma) coated glass
116 coverslips for immunostaining (100K cells per well in 24-well plates) or PDL coated
117 tissue-culture plates (3M cells per 10 cm plate) for cell fractionation experiments.
118
119 **Cloning:** The *Prmt8* transcript was amplified from mouse hippocampal cDNA using
120 the primers F: 5'-TGCTCTAGAGCAGAAGTTGGGAGAGTTGC-3' and R: 5'-
121 AGAGCGATCGCACGCATTTTGTAGTCATT-3'. The amplified region spanned from
122 base pairs 29 to 1594 of the *Prmt8* transcript (NM_201371.2) including the coding
123 sequence and most of the 5'UTR (to mimic *in vivo* start codon selection to the extent
124 possible). The *Prmt8* PCR product was digested and cloned into a derivative of the
125 FUGW lentiviral **plasmid** (Lois et al., 2002) upstream of, and in frame with, 3 X
126 FLAG and 2 X HA tags.
127
128 **Bioinformatics:** The dataset of gene expression from sorted cortical excitatory
129 (pyramidal) and inhibitory (vasoactive intestinal peptide and parvalbumin positive)
130 neurons was from GSE63137. For RNA-Seq data, single-end sequencing reads were
131 mapped to the mouse genome with GENCODE vM9 using STAR. Processed RNA-seq
132 data are available at http://bioinfo5pilm46.mit.edu:318/neugene/
133
134 **Immunostaining and imaging:** Primary neurons grown on coverslips were
135 transduced with PRMT8 expressing lentivirus at DIV5. At DIV17 the cells were fixed
136 10 min with 4% formaldehyde in 1 X PBS, washed with PBS and blocked 1 hour with
137 blocking buffer (5% donkey serum, 0.3% Triton X-100 in PBS), then stained

overnight at 4°C with primary antibodies in blocking buffer. Primary antibodies used were mouse-PSD95 (NeuroMab) and rabbit-FLAG (Santa Cruz). Primary antibodies were detected using fluorescently conjugated secondary antibodies from Jackson ImmunoResearch (anti-mouse-Cy2 and anti-rabbit-Cy5). For brain slices, mice were perfused briefly with PBS, followed by perfusion with 4% formaldehyde in PBS. Brains were removed and post fixed in 4% formaldehyde in PBS overnight at 4°C followed by storage at 4°C in PBS. 40 µm coronal sections were generated with a Leica VT1000S vibratome. Staining was performed as described above for primary neurons. Primary antibodies used were mouse-Svp38 (Sigma) and rabbit-TBR1 (Abcam). Hoechst nuclear stain was added during secondary staining together with anti-mouse-Cy2 and anti-rabbit-Cy3 (Jackson). Golgi staining was performed with the FD Rapid GolgiStain Kit (Neurotechnologies) following manufacturers instructions. Imaging was performed using a Zeiss 710 confocal microscope.

Western blotting: Western blots were performed using PVDF membranes (Millipore) following standard methods. DIV17 primary neurons infected with PRMT8 lentivirus were used to examine PRMT8 subcellular localization. Cellular fractionation was performed following published protocols with some modifications (Chao et al., 2013). The “presynaptic” fraction is Svp38-enriched while the “postsynaptic” fraction is PSD95-enriched. “Synaptosomal” preparations from mouse hippocampi followed the same procedure and correspond to the combined presynaptic plus postsynaptic fractions. Antibodies used include: mouse-PSD95 (NeuroMAB), mouse-HDAC2 (Abcam), rabbit-HA (Santa Cruz), mouse-Svp38

(Sigma), rabbit-Cacna1C (Novus), mouse-Syn1 (Synaptic Systems), rabbit-Nsf-1 (Thermo Fisher), rabbit-Syn2 (Abcam), rabbit-Syn3 (Synaptic Systems), rabbit-Syt7 (Abcam), mouse-Syt12 (NeuroMAB), rabbit-Cplx1 (Proteintech), mouse-β-actin (Sigma), rabbit-NR2A (Cell Signaling), rabbit-NR2B (Cell Signaling), mouse-NR1 (Millipore), mouse-GluA1 (Millipore), rabbit-GluA2 (Cell Signaling), mouse-CaMKIIA (Chemicon), mouse-Shank1 (NeuroMAB), mouse-α-Tubulin (Sigma), rabbit-Homer (GeneTex), rabbit-eIF4G1 (Cell Signaling), rabbit-eIF4H (Cell Signaling), rabbit-eIF4E (Cell Signaling), and rabbit-FMRP (Cell Signaling).

Quantitative PCR: RNA was extracted from freshly dissected hippocampi using the QIAGEN RNeasy Plus Mini Kit. cDNA synthesis was performed with RNA to cDNA EcoDry Premix (Oligo dT) (Clonetech). qPCR was performed with SsoFast EvaGreen Supermix (Bio-Rad) using a C1000 Thermal Cycler and a C96 Real-Time System (Bio-Rad). Target genes were normalized using *Histone H2A* unless indicated.

Electrophysiology: Transverse hippocampal slices were prepared from 2-4 month-old male littermates. The brain was rapidly isolated and transferred to ice-cold, oxygenated (95% O_2 and 5% CO_2) cutting solution containing (mM) 211 sucrose, 3.3 KCl, 1.3 NaH_2PO_4, 0.5 $CaCl_2$, 10 $MgCl_2$, 26 $NaHCO_3$ and 11 glucose. Hippocampal tissue was cut with a VT1000S vibratome (Leica) and slices were transferred for recovery to a holding chamber containing oxygenated (95% O_2 and 5% CO_2) artificial cerebrospinal fluid (ACSF) consisting of (mM) 124 NaCl, 3.3 KCl, 1.3 NaH_2PO_4, 2.5 $CaCl_2$, 1.5 $MgCl_2$, 26 $NaHCO_3$ and 11 glucose at 28-30 °C for 1hr before

recording. CA1 fEPSPs evoked by Schaffer collateral stimulation were recorded using an AM-1800 Microelectrode amplifier (A-M systems) with Digidata 1440A A-D converter (Axon Instruments). LTP was induced by three episodes of theta-burst stimulation (TBS) with 10 sec intervals. TBS consisted of ten brief bursts of stimuli delivered at 5 Hz; each burst contains four pulses at 100 Hz. Whole-cell recordings were performed in CA1 pyramidal neurons as previously described (Seo et al., 2014). In brief, cells were held at -70 mV with recording pipettes containing (mM) 145 CsCl, 5 NaCl, 10 HEPES-CsOH, 10 EGTA, 4 MgATP and 0.3 Na_2GTP. TTX (1 μM) and picrotoxin (50 μM) were added to ACSF for mEPSCs measurements, and picrotoxin was replaced with CNQX (10 μM) and D-APV (50 μM) for mIPSCs measurements. For recording GluN2A-containing NMDAR-mediated current, Schaffer collateral was stimulated and recording was performed in CA1 pyramidal neurons. Cells were held at +40 mV and Glycine (10 μM), picrotoxin (50 μM), CNQX (10 μM) and Ro 25-6981 (1 μM) were added to ACSF to isolate GluN2A-containing NMDAR-mediated current. The decay weighted time constant was calculated as previously reported (Cathala et al., 2005). Recording was performed using a MultiClamp 700B amplifier and a Digidata 1440A A-D converter (Axon Instruments). All data were analyzed by the use of pClamp 10 software (Axon Instruments).

Behavior: Open Field Test: Locomotor activity in an open field arena (41 cm x 40 cm x 30 cm) was measured over a 10 min period with AccuScan Instruments VersaMax Animal Activity Monitoring System. Time spent in center, total distance,

and hyperactivity were measured using the automated monitoring system. Light-Dark Exploration Test: A testing box (41 cm x 41 cm x 30 cm) was divided into two sections of equal size with a partition that allowed for free movement from one side to the other side. One chamber was brightly illuminated, while the other chamber was dark. Mice were placed into the dark side, and measurements were taken for latency to enter the light side, total number of transitions, and total amount of time in the light chamber. Fear Conditioning Test: Mice were put in the conditioning chamber (TSE systems) for 3 min, followed by a 30 s auditory cue (3 kHz, 80 dB) after which a constant 2 s foot shock (0.8 mA) was applied. 24 hours later, mice were re-exposed to the training context for 3 minutes and their freezing behavior was scored for memory acquisition. 48 hours after the initial conditioning (training), mice were exposed to a novel context during which they were habituated to the novel context for 2 min, followed by a 2 min auditory cue (3 kHz, 80 dB) identical to that from training session, and their freezing behavior was scored for memory acquisition.

Experimental Design and Statistical Analysis: Data are expressed as means +/- SEM or percentage and were analyzed by Excel software (Microsoft). Student's *t* test was used to analyze the means and $p </= 0.05$ was considered significant.

Results

PRMT8 is a synaptic protein

During mass spectrometry-based proteomic experiments using mouse brain tissue (Su et al., 2012), we noted that several members of the PRMT protein family were found in synaptosomal preparations from wild-type mouse cortex (Figure 1a). Among these, PRMT8 was most enriched, showing similar abundance to a number of well-established synaptic proteins (Figure 1a). Combined with the observation that many synaptic proteins are arginine methylated (Guo et al., 2014), these findings prompted us to examine a role for PRMT8 in regulating synaptic function in more detail. The synaptosomal preparations used for proteomic screening contain both pre- and postsynaptic membrane, thus we sought to test whether PRMT8 localizes specifically to one compartment or the other (or both). Available PRMT8 antibodies do not show a specific signal by western blot or immunostaining (data not shown), so we generated a lentiviral construct to express PRMT8 C-terminally tagged with FLAG and HA (see methods). Following expression of this construct in mouse primary neurons we performed subcellular fractionation to isolate nuclear, presynaptic and postsynaptic enriched fractions (Figure 1b). These experiments revealed that tagged PRMT8 is enriched in both pre- and post-synaptic fractions, and somewhat surprisingly that PRMT8 is depleted in nuclear fractions (Figure 1b). We next performed immunostaining to examine the synaptic localization of PRMT8 using mouse primary neurons expressing tagged PRMT8. Consistent with our proteomic and subcellular fractionation findings, PRMT8 signal appeared enriched in dendritic processes, and co-localized with PSD95 in dendritic spines (Figures 1 C-F). As in our subcellular fractionation experiments we did not observe strong PRMT8 signal in neuronal nuclei (data not shown). Together these findings indicate

that PRMT8 protein robustly localizes to both pre- and post-synaptic sites, and is less enriched in neuronal nuclei.

Prmt8 cKO mice develop normally

Having established that PRMT8 is a synaptic protein, we set out to characterize the effects of PRMT8 loss on brain development and function. PRMT8 is widely expressed in mouse neurons, thus we bred mice with the *Prmt8* 5th exon flanked by loxP sites (Taneda et al., 2007; Allen Institute, 2011; Skarnes et al., 2011)(Figure 2a), to mice harboring a *Nestin-cre* transgene. The *Prmt8* 5th exon encodes residues essential for methyltransferase activity, while the *Prmt8* 3rd exon contains residues required for phospholipase activity (Lee et al., 2005; Kim et al., 2015). qPCR experiments using hippocampal RNA from control (*Prmt8* floxed) and *Prmt8* cKO (*Prmt8* floxed; *Nestin-cre*) mice revealed a complete loss of *Prmt8* exon 5, as well as strong reductions in full length *Prmt8* transcript, presumably due to nonsense-mediated decay (Figure 2b). Thus, *Prmt8* cKO mice lack PRMT8 methyltransferase function and should exhibit strongly reduced phospholipase activity. We next tested whether there might be compensatory changes in the expression of other genes encoding PRMT family members in *Prmt8* cKO mice. qPCR using hippocampal RNA revealed no significant differences in expression of any PRMT family members (aside from *Prmt8*) in cKO mice compared to controls, suggesting a lack of compensatory changes in response to *Prmt8* mutation (Figure 2c).

Prmt8 cKO mice were viable and fertile, and brain weights of male and female mice did not differ between cKO and controls (Figure 2d and 2e). Similarly, we found no significant difference in cortical thickness between the two groups of mice (Figure 2f-2l). Immunostaing for the deep layer cortical marker TBR1 (T-box, brain 1) also revealed no difference in the thickness of the TBR1 layer (control: 194 +/- 13 μm; cKO: 174 +/- 4 μm. N = 9 for each; Figure 2f-2k), suggesting that *Prmt8* mutation does not affect gross cortical development. We next examined hippocampal structures in *Prmt8* cKO mice and controls finding that hippocampal thickness in area CA1 did not differ between cKO and control mice (Figure 2m-2s). We next evaluated hippocampal synapse density by immunostaining for the synaptic vesicle protein synaptophysin (Svp38), again finding no difference between cKO and control mice (Figure 2m-2r and 2t). To more closely examine neuronal morphology, we performed Golgi staining on brain slices from cKO and control mice. Quantification of dendritic spines on pyramidal neurons revealed no difference in total spine density in control vs. cKO mice (Figure 2u-2w). Similarly, an analysis of dendritic spine morphologies revealed no significant differences in the proportion of “mushroom”, “thin” or “stubby” spines between *Prmt8* cKO and control mice (Figure 2u-2x). Together, these findings indicate that neither overall forebrain development nor hippocampal synapse density or dendritic spine morphology are altered by *Prmt8* mutation.

PRMT8 mutation alters synaptic function and plasticity

We next sought to examine whether *Prmt8* mutation affects neuronal function and/or synaptic plasticity in the hippocampus. To test this possibility, we performed field potential recordings from area CA1 of hippocampal slices from *Prmt8* cKO mice and controls. Input-output curves generated following stimulation of Schaffer collaterals revealed an increased field EPSP (fEPSP) slope in slices from *Prmt8* cKO mice, indicating an increase in baseline synaptic transmission (Figure 3a and 3b). We next measured the paired-pulse facilitation (PPF) ratio at Schaffer collateral-CA1 synapses, finding that *Prmt8* cKO slices exhibited a reduced PPF ratio (Figure 3c). This reduced PPF ratio suggests that *Prmt8* mutation results in an increased probability of presynaptic neurotransmitter release. We then tested whether long-term potentiation (LTP) of Schaffer collateral-CA1 synapses was altered by *Prmt8* mutaion. We found that while 3 X TBS (theta-burst stimulation) did induce LTP in slices from *Prmt8* cKO mice, its magnitude was significantly reduced compared to control slices (Figure 3d and 3e). Thus, *Prmt8* mutation appears to increase evoked neurotransmitter release at Schaffer collateral-CA1 synapses, while also reducing long-term synaptic plasticity induced by TBS.

We next sought to test whether miniature synaptic transmission was affected by *Prmt8* mutation. We first verified that *Prmt8* was expressed in both excitatory and inhibitory neurons *in vivo* utilizing publically available cell type-specific gene expression data (Mo et al., 2015; also available at http://bioinfo5pilm46.mit.edu:318/neugene/). While this data showed strong expression of *Rbfox3* (encoding NeuN) in both excitatory and inhibitory neurons,

and the expected enrichments of *Slc17a7* (encoding VGlut1) and *Gad1* (encoding Gad67) in excitatory or inhibitory neurons, respectively, we found that *Prmt8* expression was almost identical in the two neuronal sub-types (Figure 4a-4d).

Thus we proceeded to perform intracellular recordings from CA1 pyramidal neurons to measure spontaneous miniature EPSCs (mEPSCs). Typically, changes in mEPSC frequency are taken to reflect differences in synapse number and/or probability of presynaptic release, while altered mEPSC amplitudes are most often due to altered postsynaptic neurotransmitter receptor levels or function. Our analysis of intracellular recordings in *Prmt8* cKO vs. control slices revealed a significant ~15% increase in mEPSC amplitudes, as well as a more than tripling of mEPSC frequency in neurons lacking functional PRMT8 (Figure 4e-4i). This large increase in mEPSC frequency was surprising considering we did not observe any differences in synaptophysin staining intensity (Figure 2m-2t) or dendritic spine density (Figure 2u-2x), though it is consistent with the increased baseline transmission and reduced PPF values we observed in *Prmt8* cKO mice. Thus the elevated mEPSC frequency may reflect an alteration in synaptic vesicle dynamics or recycling resulting in an increase in presynaptic neurotransmitter release. Regardless, these findings indicate that *Prmt8* cKO mice exhibit considerable defects affecting both pre- and post-synaptic excitatory neuronal function and plasticity.

We next measured spontaneous miniature IPSCs (mIPSCs) from CA1 pyramidal neurons. In contrast to the striking alterations in mEPSC amplitude and frequency

342 we observed, we found no significant differences in mIPSC amplitude or frequency
343 when comparing slices from control and *Prmt8* cKO mice (Figure 4j-4n). Thus,
344 despite the reported defects in inhibitory neuron structures in the visual cortex (Lee
345 et al., 2017), and the differences in excitatory synaptic function just described, we
346 did not detect any alterations due to *Prmt8* mutation in miniature inhibitory
347 currents received by hippocampal pyramidal neurons.
348
349 ***PRMT8 post-transcriptionally regulates synaptic proteins***
350 Given the effects we observed following *Prmt8* mutation on synaptic function and
351 plasticity, we next sought to test whether synaptic protein composition was altered
352 in *Prmt8* cKO mice. To address this possibility we examined the levels of a panel of
353 pre- and post-synaptic proteins both in hippocampal lysates from *Prmt8* cKO mice
354 and controls, as well as in synaptosomal preparations from these mice. We found no
355 change in the synaptic levels of the voltage-gated calcium channel subunit Cacna1C,
356 which we were unable to detect in total lysates (Figure 5a). Similarly we found no
357 differences in the total or synaptic levels of the synaptic vesicle proteins Synapsin 1
358 (Syn1), Synapsin 2 (Syn2), Synapsin 3 (Syn3) and Synaptophysin (Svp38), or the
359 presynaptic regulators *N*-ethylmaleimide-sensitive factor (Nsf-1), Synaptotagmin 7
360 (Syt7), Synaptotagmin 12 (Syt12) and Complexin 1 (Cplx1) when comparing control
361 to cKO mice (Figure 5a). We next examined a number of glutamate receptor
362 subunits and signaling proteins, finding no change in levels of the AMPA receptor
363 subunits GluA1 and GluA2, the NMDA receptor subunits GluN1 and GluN2B, or the
364 synaptic signaling molecule CaMKII, in either total or synaptosomal lysates (Figure

5b). In contrast, we did find a significant reduction in levels of the NMDA receptor subunit GluN2A in both total lysates and synaptic fractions (Figure 5b), suggesting that NMDA receptor function could be altered in *Prmt8* cKO mice. We next examined a number of synaptic and cellular scaffolding proteins, finding no significant change in the total or synaptosomal levels of cytoskeletal component α-Tubulin or the synaptic scaffolding proteins Shank 1, PSD95 and Homer (Figure 5c). We also examined levels of the RNA-binding protein FMRP and a number of cap-dependent translation regulators as these proteins are important for synaptic plasticity, and many are arginine methylated in the mouse brain (Guo et al., 2014), suggesting the possibility they could be regulated by PRMT8. While we did not detect changes in FMRP levels in total or synaptic fractions, we did find reduced levels, or trends to reduced levels, in the eukaryotic initiation factors (eIFs) eIF4G1, eIF4H and eIF4E in both total and synaptic fractions from *Prmt8* cKO mice (Figure 5d). Thus, a number of synaptic plasticity-related proteins exhibit altered expression following *Prmt8* mutation.

We next tested whether the mRNA levels corresponding to a number of synaptic proteins, including those we found reduced at the protein level, were altered in *Prmt8* cKO mice. Consistent with their unaltered protein levels we found no difference in the expression of mRNAs encoding GluA1, PSD95 or CaMKIIA (Figure 5e). Intriguingly we also found no difference in the expression of mRNAs encoding GluN2A, eIF4G1, eIF4H and eIF4E, despite their reduced protein levels in *Prmt8* cKO mice (Figure 5e). We further examined the mRNA levels of *cFos*, *Npas4* and *Egr1*,

three immediate early genes important for synaptic plasticity, and again found no significant difference between cKO vs. control mice (Figure 5e). Thus, we did not detect any differences in the transcript levels of numerous proteins involved in synaptic function and plasticity. Importantly, the discordance of mRNA and protein levels for GluN2A, eIF4G1, eIF4H and eIF4E indicates that post-transcriptional mechanisms appear to be involved in the reduced levels of these proteins following mutation of PRMT8.

mRNA transport to synaptic sites and localized mRNA translation are important mechanisms in synaptic plasticity (Holt and Schuman, 2013). PRMT8 can physically interact with a number of RNA-binding proteins, and numerous RNA binding proteins such as FMRP are arginine methylated in the mouse brain (Pahlich et al., 2008; Guo et al., 2014). Thus, we sought to test whether synaptic mRNA localization could be altered in *Prmt8* cKO mice. To test this we isolated mRNA from hippocampal synaptosomal preparations and compared enrichment of specific mRNAs in these samples to total hippocampal mRNA from the same animals. Using equivalent amounts of total and synaptosomal RNA we found that as expected *GAPDH* and histone *H2A* mRNAs were depleted in synaptic samples vs. total RNA (54 +/- 2% and 63 +/- 6%, respectively). In contrast, known synaptically localized mRNAs such as *PSD95*, *Arc* (encoding Activity-regulated cytoskeletal protein) and *CaMKII* (Burgin et al., 1990; Steward et al., 1998; Zalfa et al., 2007) were enriched in synaptic vs. total mRNA (147 +/- 23%, 207 +/- 16% and 212 +/- 16%, respectively). Next we compared the synaptic enrichment, normalized to *GAPDH*, of these and

411 other transcripts from control and *Prmt8* cKO mice (Figure 5f). We found no
412 difference in the synaptic enrichment of *H2A*, *FMRP*, *PSD95*, *Arc*, *CaMKII* or *MAP1B*
413 (encoding microtubule associated protein 1B) mRNAs (Figure 5f), suggesting that
414 PRMT8 is not required for proper mRNA localization to synaptic sites.
415
416 ***GluN2A-mediated currents are reduced in PRMT8 cKO mice***
417 The reduction in GluN2A protein levels we observed in hippocampal lysates from
418 *Prmt8* cKO mice prompted us to test whether we could also detect functional
419 alterations in NMDAR function. Thus we measured evoked GluN2A currents in CA1
420 pyramidal neurons from control and *Prmt8* cKO slices. Consistent with the reduced
421 GluN2A protein levels we observed in *Prmt8* mutant hippocampi, GluN2A-mediated
422 NMDAR currents were also strongly reduced compared to controls (Figure 6a and
423 6b). We also calculated the decay time of GluN2A-mediated currents from control
424 and cKO mice. While we found a trend towards increased decay time of GluN2A-
425 mediated currents from *Prmt8* cKO slices, it was not significantly different from
426 controls suggesting that the main effect may is due to reduced GluN2A levels rather
427 than altered kinetics (Figure 6c).
428
429 ***PRMT8 cKO mice exhibit deficits in contextual fear memory***
430 Finally, we undertook a behavioral analysis of *Prmt8* cKO mice to examine the
431 potential effects on cognitive processes that might arise from the synaptic protein
432 and synaptic functional defects that we uncovered in these mice. We found no
433 difference between control and cKO mice in total distance travelled in the open field

arena (Figure 7a). Similarly, we observed no significant differences in the proportions of time control and cKO mice spent in the center vs. periphery of the open field arena, suggesting anxiety-related behaviors were not altered by *Prmt8* mutation (Figures 7b and 7c). Also consistent with normal anxiety-related behaviors, control and cKO mice did not differ in the amount of time spent in light, the number of visits to light, or the latency to visit light in the light/dark test (Figures 7d-7f). We next assayed fear learning and memory using a classical fear-conditioning paradigm. Mice were habituated to a chamber, and then an audible tone was paired with an aversive foot shock. Typically, mice will learn to associate both the chamber (context) and the tone (cue) with the foot shock. 24 hours later the mice were returned to the same chamber and the percent of time they spent freezing (without tone or foot shock) was quantified as a measure of context-dependent fear memory. A further 24 hours later the mice were placed in a distinct chamber and played the tone that was initially paired with foot shock; the percent of time spent freezing was again quantified, this time as a measure of cued fear memory. These experiments revealed no difference in freezing by *Prmt8* cKO mice compared to controls in response to tone (Figure 7g), but significantly less freezing by cKO mice when returned to the training chamber (Figure 7h). Thus, mutation of *Prmt8* results in a specific deficit in contextual fear memory, consistent with altered hippocampal function.

Discussion

Here we have established that PRMT8 is a synaptic protein, and characterized hippocampal synaptic structures, protein content and electrophysiological function, as well as examining behavioral function in *Prmt8* cKO mice. We find that while synapse and dendritic spine density are unaltered, mutation of *Prmt8* does affect multiple measures of neuronal function, synaptic protein composition and hippocampal-dependent fear learning. These findings clearly demonstrate that PRMT8 is required for normal hippocampal function of the mammalian brain.

Our most striking findings were that multiple excitatory synaptic functional parameters were altered by *Prmt8* mutation. Input-output curves of field potentials following stimulation of Schaffer collaterals indicated an increase in baseline synaptic transmission in *Prmt8* cKO slices. Consistently, paired pulse facilitation ratios were reduced in slices from cKO mice. In addition, intracellular recordings revealed an elevation in both mEPSC amplitudes and frequencies, perhaps underlying the increased baseline synaptic function we observed. We furthermore observed deficits in GluN2A-mediated NMDAR currents in *Prmt8* cKO slices. In contrast, we found that mIPSC properties were not altered by *Prmt8* mutation, indicating that PRMT8 has distinct effects in different neuronal subtypes.

The large increase we observed in mEPSC frequencies was surprising considering that synapse density (as assayed by synaptophysin staining) and dendritic spine density were both unaltered in *Prmt8* cKO mice. Together these observations suggest an alteration in the synaptic vesicle release machinery in cKO mice, though

we did not detect any differences in proteins involved in presynaptic release in our synaptic protein analysis. Similarly we did not detect any increases in AMPA receptor proteins that would be consistent with elevated mEPSC amplitudes in *Prmt8* cKO mice. In conjunction with these alterations in synaptic function, we also observed reduced LTP induction in cKO mice. It is possible that elevated baseline transmission in the cKO mice partially occludes LTP induction, however other mechanisms such as the impaired NMDAR signaling we observe, could also result in defective long-term synaptic plasticity following *Prmt8* mutation. Further experiments will be required to distinguish between these possibilities. Regardless, multiple aspects of pre- and post-synaptic excitatory function are affected in mice lacking functional PRMT8 protein.

In addition to reduced GluN2A levels, we also observed reductions in multiple members (eIF4E, eIF4G1 and eIF4H) of the mRNA cap-binding complex, required for translation of most mRNAs in eukaryotic cells (Sonenberg and Hinnebusch, 2009). Despite the requirement of this protein complex for global cellular protein synthesis, alterations in cap-binding complex activity are an important regulator of synaptic function, plasticity and behavior (Banko et al., 2005; Penney et al., 2012; Gkogkas et al., 2013). Importantly, changes in cap-binding complex function can selectively affect certain mRNAs based on sequences or structural elements in their untranslated regions (Sonenberg and Hinnebusch, 2009). Furthermore, ribosomes, cap-binding complex proteins and specific mRNAs also localize to postsynaptic sites in the nervous system, allowing for rapid, activity-dependent translation of key

synaptic proteins (Holt and Schuman, 2013). Together these mechanisms can allow modest and/or localized changes in cap-binding complex function to affect synaptic plasticity but not global protein synthesis. Intriguingly, the *GluN2A* mRNA has been shown to possess upstream open reading frames and secondary structure elements in its 5'UTR that inhibit translation of the protein coding open reading frame (Wood et al., 1996). Thus, it is possible that the observed decrease in GluN2A protein could be due to inefficient translation resulting from reduced cap-binding complex function in *Prmt8* cKO mice, though this idea requires direct testing. The observed reduction in cap-binding complex proteins could also affect synaptic function and plasticity in cKO mice via additional target mRNAs, as well as by potentially inhibiting activity-induced synaptic protein synthesis.

Whether the reduced GluN2A levels and function in *Prmt8* cKO mice are due to perturbed translation or other mechanisms, they have the potential to contribute to multiple cellular and behavioral phenotypes we describe in these mice. GluN2A-containing NMDARs are important modulators of hippocampal LTP, and mice harboring *GluN2A* mutations have multiple behavioral defects including impaired contextual fear learning (Sakimura et al., 1995; Sprengel et al., 1998). Thus, despite unaltered levels of GluN1 and GluN2B, reduced levels of GluN2A in *Prmt8* cKO mice may make important contributions to their altered synaptic and cognitive function.

The multiple neuronal function alterations we describe following *Prmt8* mutation are accompanied by a deficit in contextual fear memory, while the other behavioral

parameters we tested were not significantly different between control and cKO mice. Control and cKO mice traveled a similar distance in the open field, suggesting no difference in activity levels. This finding is in contrast to Kim et al., (2015), who reported a hyperactivity phenotype in whole body *Prmt8* cKO mice (using the *Ayu1-cre* driver). We used the neural lineage-specific *Nestin-cre* to conditionally delete *Prmt8*, however since *Prmt8* is expressed almost exclusively in neurons (Lee et al., 2005; Zhang et al., 2014) it is not clear how use of these different cre drivers would affect locomotor activity. We also did not observe a hind-limb clasping phenotype in cKO mice as reported by Kim et al., (2015) (data not shown). Our behavioral analysis further examined anxiety-related phenotypes in *Prmt8* cKO mice, indicating that *Prmt8* mutation does not appear to alter anxiety-related behaviors. Finally we tested both cued and context-dependent fear memory in cKO mice and controls. While we did not observe significantly reduced freezing behavior in response to a cue associated with foot shock, we did find that *Prmt8* cKO mice froze less in the training context that was associated with foot shock. As contextual fear learning is a hippocampal-dependent process, these results are consistent with a deficit in hippocampal cognitive function following mutation of *Prmt8*.

In the current study we focused on phenotypes in hippocampal pyramidal neurons resulting from *Prmt8* mutation, however, PRMT8 has been reported to affect other neuron types and brain regions as well. Kim et al. (2015) reported that *Prmt8* mutation impaired cerebellar Purkinje neuron branching, as well as reducing the levels of choline and acetylcholine in the cerebellum. In addition, Lee et al. (2017)

548 found that *Prmt8* mutation increased perineuronal net formation around
549 parvalbumin (PV)-positive interneurons of the visual cortex, associated with
550 increased PV neuron complexity and reduced visual acuity. Thus it is possible that
551 altered cholinergic or GABAergic function in *Prmt8* cKO mouse brains could
552 contribute to the defects in hippocampal synaptic plasticity and behavior we
553 describe here. Further experiments will be required to test these possibilities.
554
555 PRMT8 is a multifunctional protein possessing both arginine methyltransferase and
556 phospholipase activities (Lee et al., 2005; Kim et al., 2015). The relative contribution
557 of these enzymatic functions to *Prmt8* cKO phenotypes remains an open question.
558 While few endogenous PRMT8 methylation targets have been identified, many
559 synaptic proteins are arginine methylated in the mouse brain (Guo et al., 2014).
560 These include a number of proteins examined in our analysis (Syn1, Syn3, Syt7,
561 eIF4G1, eIF4H and FMRP), however determining whether PRMT8 regulates the
562 methylation of these proteins, and what effects that methylation would have on
563 protein function, will require further analysis. It is interesting to note that multiple
564 members of the mRNA cap-binding complex, whose levels we found reduced in
565 *Prmt8* cKO mice, are methylation targets. Potentially arginine methylation of these
566 proteins could regulate their stability, or otherwise regulate the formation and/or
567 function of the cap-binding complex. Also noteworthy was our observation that only
568 a minority of tagged PRMT8 protein localized to the nucleus. Multiple PRMT
569 enzymes are well-characterized epigenetic regulators of gene expression (Bedford
570 and Clarke, 2009) and some studies have implicated PRMT8 in similar mechanisms

(Kousaka et al., 2009; Simandi et al., 2015; Lee et al., 2017). Our observation that the proteins we found reduced in *Prmt8* cKO mice did not exhibit parallel reductions in their mRNA levels, and that PRMT8 itself localizes to synaptic sites, suggest that PRMT8 likely plays important non-nuclear roles in neurons, though we do not rule out additional nuclear functions for PRMT8.

PRMT8-dependent phospholipase D activity could also regulate brain function in multiple ways. Phospholipase D enzymes catalyze the conversion of phosphatidylcholine (PC) into phosphatidic acid (PA) and choline, with the latter serving as the substrate for acetylcholine metabolism (Klein, 2005). As noted, *Prmt8* knockout mice were reported to have reduced cerebellar choline and acetylcholine levels, as well as increased PC content (Kim et al., 2015). Alterations of both cholinergic neurotransmission and the catabolism of PC, a major phospholipid component of biological membranes, have the potential to affect hippocampal function. Thus, the methyltransferase and phospholipase activities of PRMT8 may synergistically contribute to the phenotypes of *Prmt8* cKO mice.

Together our findings establish PRMT8 as a constituent of the synaptic proteome with important roles in the nervous system. PRMT8 post-transcriptionally modulates the levels of a number of proteins important for synaptic plasticity, and *Prmt8* cKO mice exhibit multiple alterations in hippocampal synaptic function and plasticity. These alterations in synaptic function occur without detectable changes brain or neuron morphology, and are accompanied by impairment in hippocampal-

dependent fear memory. Our findings establish PRMT8 as an important component of the molecular machinery regulating synaptic physiology, and reveal novel roles for this protein in hippocampal function.

References

Allen Institute for Brain Science. (2011) Mouse Reference Atlas, Version 2. Available from: mouse.brain-map.org.

Banko JL, Poulin F, Hou L, DeMaria CT, Sonenberg N, Klann E (2005) The translation repressor 4E-BP2 is critical for eIF4F complex formation, synaptic plasticity, and memory in the hippocampus. J Neurosci 25:9581-9590.

Bedford MT, Clarke SG (2009) Protein arginine methylation in mammals: who, what, and why. Mol Cell 33:1-13.

Burgin KE, Waxham MN, Rickling S, Westgate SA, Mobley WC, Kelly PT (1990) In situ hybridization histochemistry of Ca2+/calmodulin-dependent protein kinase in developing rat brain. J Neurosci 10:1788-1798.

Burkhardt U, Stegner D, Hattingen E, Beyer S, Nieswandt B, Klein J (2014) Impaired brain development and reduced cognitive function in phospholipase D-deficient mice. Neurosci Lett 572:48-52.

Cathala L, Holderith NB, Nusser Z, DiGregorio DA, Cull-Candy SG (2005) Changes in synaptic structure underlie the developmental speeding of AMPA receptor-mediated EPSCs. Nat Neurosci 8:1310-1318.

Chao HW, Tsai LY, Lu YL, Lin PY, Huang WH, Chou HJ, Lu WH, Lin HC, Lee PT, Huang YS (2013) Deletion of CPEB3 enhances hippocampus-dependent memory via increasing expressions of PSD95 and NMDA receptors. J Neurosci 33:17008-17022.

Gkogkas CG, Khoutorsky A, Ran I, Rampakakis E, Nevarko T, Weatherill DB, Vasuta C, Yee S, Truitt M, Dallaire P, Major F, Lasko P, Ruggero D, Nader K, Lacaille JC,

620 Sonenberg N (2013) Autism-related deficits via dysregulated eIF4E-
621 dependent translational control. Nature 493:371-377.
622 Guo A, Gu H, Zhou J, Mulhern D, Wang Y, Lee KA, Yang V, Aguiar M, Kornhauser J, Jia
623 X, Ren J, Beausoleil SA, Silva JC, Vemulapalli V, Bedford MT, Comb MJ (2014)
624 Immunoaffinity enrichment and mass spectrometry analysis of protein
625 methylation. Mol Cell Proteomics 13:372-387.
626 Holt CE, Schuman EM (2013) The central dogma decentralized: new perspectives on
627 RNA function and local translation in neurons. Neuron 80:648-657.
628 Kandel ER (2001) The molecular biology of memory storage: a dialogue between
629 genes and synapses. Science 294:1030-1038.
630 Kim JD, Park KE, Ishida J, Kako K, Hamada J, Kani S, Takeuchi M, Namiki K, Fukui H,
631 Fukuhara S, Hibi M, Kobayashi M, Kanaho Y, Kasuya Y, Mochizuki N,
632 Fukamizu A (2015) PRMT8 as a phospholipase regulates Purkinje cell
633 dendritic arborization and motor coordination. Sci Adv 1:e1500615.
634 Klein J (2005) Functions and pathophysiological roles of phospholipase D in the
635 brain. J Neurochem 94:1473-1487.
636 Kousaka A, Mori Y, Koyama Y, Taneda T, Miyata S, Tohyama M (2009) The
637 distribution and characterization of endogenous protein arginine N-
638 methyltransferase 8 in mouse CNS. Neuroscience 163:1146-1157.
639 Lee J, Sayegh J, Daniel J, Clarke S, Bedford MT (2005) PRMT8, a new membrane-
640 bound tissue-specific member of the protein arginine methyltransferase
641 family. J Biol Chem 280:32890-32896.

642 Lee PK, Goh WW, Sng JC (2017) Network-based characterization of the synaptic
643 proteome reveals that removal of epigenetic regulator Prmt8 restricts
644 proteins associated with synaptic maturation. J Neurochem 140:613-628.
645 Lois C, Hong EJ, Pease S, Brown EJ, Baltimore D (2002) Germline transmission and
646 tissue-specific expression of transgenes delivered by lentiviral vectors.
647 Science 295:868-872.
648 Mo A, Mukamel EA, Davis FP, Luo C, Eddy SR, Ecker, JR, Nathans J. (2015)
649 Epigenomic Signatures of Neuronal Diversity in the Mammalian Brain.
650 Neuron 86(6):1369-84.
651 Pahlich S, Zakaryan RP, Gehring H (2008) Identification of proteins interacting with
652 protein arginine methyltransferase 8: the Ewing sarcoma (EWS) protein
653 binds independent of its methylation state. Proteins 72:1125-1137.
654 Penney J, Tsurudome K, Liao EH, Elazzouzi F, Livingstone M, Gonzalez M, Sonenberg
655 N, Haghighi AP (2012) TOR is required for the retrograde regulation of
656 synaptic homeostasis at the Drosophila neuromuscular junction. Neuron
657 74:166-178.
658 Sakimura K, Kutsuwada T, Ito I, Manabe T, Takayama C, Kushiya E, Yagi T, Aizawa S,
659 Inoue Y, Sugiyama H, et al. (1995) Reduced hippocampal LTP and spatial
660 learning in mice lacking NMDA receptor epsilon 1 subunit. Nature 373:151-
661 155.
662 Seo J, Giusti-Rodriguez P, Zhou Y, Rudenko A, Cho S, Ota KT, Park C, Patzke H,
663 Madabhushi R, Pan L, Mungenast AE, Guan JS, Delalle I, Tsai LH (2014)

664 Activity-dependent p25 generation regulates synaptic plasticity and Abeta-
665 induced cognitive impairment. Cell 157:486-498.
666 Simandi Z, Czipa E, Horvath A, Koszeghy A, Bordas C, Poliska S, Juhasz I, Imre L,
667 Szabo G, Dezso B, Barta E, Sauer S, Karolyi K, Kovacs I, Hutoczki G, Bognar L,
668 Klekner A, Szucs P, Balint BL, Nagy L (2015) PRMT1 and PRMT8 regulate
669 retinoic acid-dependent neuronal differentiation with implications to
670 neuropathology. Stem Cells 33:726-741.
671 Skarnes WC, Rosen B, West AP, Koutsourakis M, Bushell W, Iyer V, Mujica AO,
672 Thomas M, Harrow J, Cox T, Jackson D, Severin J, Biggs P, Fu J, Nefedov M, de
673 Jong PJ, Stewart AF, Bradley A (2011) A conditional knockout resource for
674 the genome-wide study of mouse gene function. Nature 474:337-342.
675 Sonenberg N, Hinnebusch AG (2009) Regulation of translation initiation in
676 eukaryotes: mechanisms and biological targets. Cell 136:731-745.
677 Sprengel R, Suchanek B, Amico C, Brusa R, Burnashev N, Rozov A, Hvalby O, Jensen
678 V, Paulsen O, Andersen P, Kim JJ, Thompson RF, Sun W, Webster LC, Grant SG,
679 Eilers J, Konnerth A, Li J, McNamara JO, Seeburg PH (1998) Importance of the
680 intracellular domain of NR2 subunits for NMDA receptor function in vivo.
681 Cell 92:279-289.
682 Steward O, Wallace CS, Lyford GL, Worley PF (1998) Synaptic activation causes the
683 mRNA for the IEG Arc to localize selectively near activated postsynaptic sites
684 on dendrites. Neuron 21:741-751.

685 Su SC, Seo J, Pan JQ, Samuels BA, Rudenko A, Ericsson M, Neve RL, Yue DT, Tsai LH
686 (2012) Regulation of N-type voltage-gated calcium channels and presynaptic
687 function by cyclin-dependent kinase 5. Neuron 75:675-687.
688 Taneda T, Miyata S, Kousaka A, Inoue K, Koyama Y, Mori Y, Tohyama M (2007)
689 Specific regional distribution of protein arginine methyltransferase 8
690 (PRMT8) in the mouse brain. Brain Res 1155:1-9.
691 Tronche F, Kellendonk C, Kretz O, Gass P, Anlag K, Orban PC, Bock R, Klein R, Schutz
692 G (1999) Disruption of the glucocorticoid receptor gene in the nervous
693 system results in reduced anxiety. Nat Genet 23:99-103.
694 Vooijs M, van der Valk M, te Riele H, Berns A (1998) Flp-mediated tissue-specific
695 inactivation of the retinoblastoma tumor suppressor gene in the mouse.
696 Oncogene 17:1-12.
697 Wood MW, VanDongen HM, VanDongen AM (1996) The 5'-untranslated region of
698 the N-methyl-D-aspartate receptor NR2A subunit controls efficiency of
699 translation. J Biol Chem 271:8115-8120.
700 Zalfa F, Eleuteri B, Dickson KS, Mercaldo V, De Rubeis S, di Penta A, Tabolacci E,
701 Chiurazzi P, Neri G, Grant SG, Bagni C (2007) A new function for the fragile X
702 mental retardation protein in regulation of PSD-95 mRNA stability. Nat
703 Neurosci 10:578-587.
704 Zhang Y, Chen K, Sloan SA, Bennett ML, Scholze AR, O'Keeffe S, Phatnani HP,
705 Guarnieri P, Caneda C, Ruderisch N, Deng S, Liddelow SA, Zhang C, Daneman
706 R, Maniatis T, Barres BA, Wu JQ (2014) An RNA-sequencing transcriptome

707 and splicing database of glia, neurons, and vascular cells of the cerebral
708 cortex. J Neurosci 34:11929-11947.
709
710

711 **Figure Legends**

712 **Figure 1:** PRMT8 localizes to synaptic sites. (A) Selected proteins from mass
713 spectrometry analysis of the synaptosomal proteome of wild-type mouse cortex.
714 The names, molecular weight (MW), number of unique peptides identified, and total
715 intensity are indicated. (B) Western blot of nuclear, presynaptic and postsynaptic
716 density (PSD) fractions from DIV17 mouse primary neurons expressing tagged
717 PRMT8 probed with antibodies recognizing the PSD protein PSD95, the nuclear
718 protein HDAC2 and the synaptic vesicle protein Svp38, as well as HA to detect
719 PRMT8. Equivalent cellular proportions of each fraction were loaded for direct
720 comparison between the fractions. Molecular weights are indicated. (C-F)
721 Immunostaining of DIV17 mouse primary neurons expressing tagged PRMT8 and
722 stained with antibodies against FLAG and the postsynaptic marker PSD95. Neurons
723 expressing an empty vector act as a control for the specificity of FLAG staining. Scale
724 bar = 10 μm.
725
726 **Figure 2:** Brain development in *Prmt8* cKO mice. (A) Schematic of the *Prmt8*
727 transcript indicating the locations of important domains and residues of the
728 encoded protein. Blue boxes indicate exons. Red triangles indicate the location of
729 *loxP* sites mediating conditional deletion of exon 5. N-myristoyl indicates the glycine
730 residue that can be N-myristoylated for membrane targeting. SH3-binding indicates
731 residues involved in interactions with SRC homology 3 domains. SAM-binding
732 indicates S-Adenosyl methionine-binding residues. (B) qPCR from hippocampal
733 mRNA of control (*Prmt8* floxed) and cKO (*Prmt8* floxed; *Nestin-cre*) mice using

primers specific to the indicated *Prmt8* exons. N = 3 for each. (C) qPCR from hippocampal mRNA of control and cKO mice using primers specific to each PRMT family member. N = 4 for each. (D) Brain weights of female mice measured following dissection of unfixed tissue. N = 8 for each. (E) Brain weights of male mice measured following perfusion and dissection of fixed brains. N = 6 for each. (F) to (K) Immunostaining of cortical slices stained with Hoechst and the deep layer cortical marker TBR1. (L) Quantification of cortical thickness above hippocampal area CA1. N = 9 for each. Scale bar = 100 μm. (M) to (R) Immunostaining of hippocampal area CA1 of mice stained with Hoechst and synaptophysin (Svp38). Scale bar = 50 μm. (S) Quantification of the density of nuclei in the molecular layer of hippocampal area CA1. N = 9 each. (T) Quantification of the synaptophysin staining intensity in hippocampal area CA1. N = 8 and 9, respectively. (U) and (V) Images of Golgi stained pyramidal neurons from hippocampal area CA1. Scale bar = 5 μm. (W) Quantification of the density of all dendritic spines corresponding to (U) and (V). N = 18 for each. (X) Quantification of the proportion of mushroom, thin or stubby dendritic spines corresponding to (U) and (V). N = 18 for each. *** $p < 0.001$ by student's t-test. Error bars +/- SEM.

Figure 3: Electrophysiological function is altered in *Prmt8* cKO mice. (A) Traces and input-output curves from control and *Prmt8* cKO mice derived by plotting the slopes of evoked fEPSPs against fiber-volley amplitude. (B) Quantification of fEPSP slopes. N = 9 for each. (C) Traces and paired-pulse facilitation ratios at the indicated interstimulus intervals. N = 9 and 11, respectively. (D) LTP induced by 3 X TBS in

slices from control and *Prmt8* cKO mice. Sample traces represent fEPSP at 1min before (gray) and 1hr after (black) TBS. (E) Quantification of LTP induction as a percent of baseline transmission from 50-60 minutes after 3 X TBS. N = 7 and 10 for control and cKO.

Figure 4: *Prmt8* mutation alters mEPSC but not mIPSC properties. FPKM (Fragments Per Kilobase of transcript per Million mapped reads) values for (A) *Rbfox3* (NeuN), (B) *Slc17a7* (VGlut1), (C) *Gad1* (Gad67) and (D) *Prmt8* from sorted mouse cortical excitatory and inhibitory neurons (based on Ma et al., 2015). (E) Traces of mEPSC activity from intracellular recordings of pyramidal neurons. (F) Quantification of average mEPSC amplitudes and (H) cumulative probability curves from control and cKO slices. N = 9 and 8, respectively. (G) Quantification of average mEPSC frequency and (I) cumulative probability curves of inter-event intervals from control and cKO slices. N = 10 and 8, respectively. (J) Traces of mIPSC activity from intracellular recordings of pyramidal neurons. (K) Quantification of average mIPSC amplitudes and (M) cumulative probability curves from control and cKO slices. N = 10 and 13, respectively. (L) Quantification of average mEPSC frequency and (N) cumulative probability curves of inter-event intervals from control and cKO slices. N = 10 and 13, respectively. * $p < 0.05$ and *** $p < 0.001$ by student's t-test. Error bars +/- SEM.

Figure 5: Synaptic protein alterations following loss of PRMT8. (A) to (D) Western blots from total lysate or synaptosomal preparations from hippocampi of control

and *Prmt8* cKO mice probed with antibodies against the indicated proteins. Protein molecular weight as well as the ratio of each protein, normalized to actin, in cKO vs. control samples is indicated. (A) Synaptic vesicle proteins and other regulators of presynaptic function. (B) Glutamate receptors and the signaling protein CaMKII. (C) Cytoskeletal and synaptic scaffolding proteins. (D) Translation initiation factors and mRNA binding proteins. N = 4 for all. (E) qPCR for *Prmt8* and genes encoding selected synaptic plasticity-related proteins from hippocampal mRNA of control and cKO mice. N = 3 for all. (F) qPCR comparing the ratio of selected transcripts from synaptic vs. total mRNA from control and cKO hippocampi. The established synaptically localized mRNAs encoding PSD95, Arc and CaMKII show clear enrichment in synaptic vs. total mRNA. N = 3 for all. * $p < 0.05$ and *** $p < 0.001$ by student's t-test. Error bars +/- SEM.

Figure 6: GluN2A currents are reduced in *Prmt8* cKO mice. (A) Traces and (B) quantification of GluN2A-mediated currents from control and *Prmt8* cKO mice (N = 8 and 7, respectively). (C) Quantification of decay time for GluN2A-mediated currents from control and *Prmt8* cKO mice (N = 8 and 7, respectively). ** $p < 0.01$ by student's t-test. Error bars +/- SEM.

Figure 7: *Prmt8* cKO mice exhibit impaired fear memory. (A) to (C) Activity of control and *Prmt8* cKO in the open field arena. (A) Total distance traveled, (B) percent of time spent in center and (C) percent of time spent in the periphery. N = 12 and 11, respectively for each parameter. (D) to (F) Light-dark test. (D) Total time

803 spent in light, (E) number of visits to the light and (F) latency to visit light. N = 11
804 and 10, respectively for each parameter. Percent of time spent freezing during
805 probe tests following cued (G) and contextual (H) fear conditioning of control and
806 cKO mice. N = 11 and 10, respectively for each test. * $p < 0.05$ by student's t-test.
807 Error bars +/- SEM.

Figure 1

A

Protein	MW	# Unique Pep.	Total Intensity
CaMKIIA	55	32	6.5e10
Syn1	74	34	2.1e10
PSD95	95	39	1.4e10
Shank1	225	74	4.6e9
GluR1	102	68	1.6e9
Syt7	51	14	4.2e8
Arc	45	15	9.9e7
FMRP	71	6	4.2e7
PRMT1	43	7	1.5e7
PRMT5	73	2	7.9e5
PRMT8	45	16	1.3e8

B

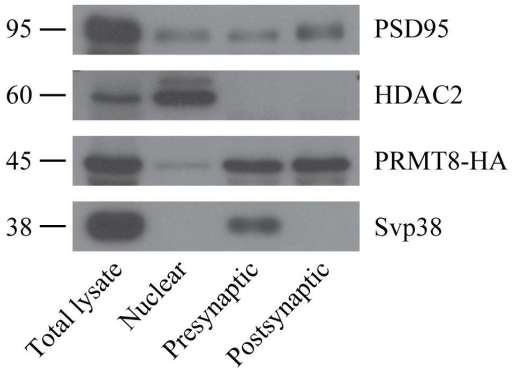

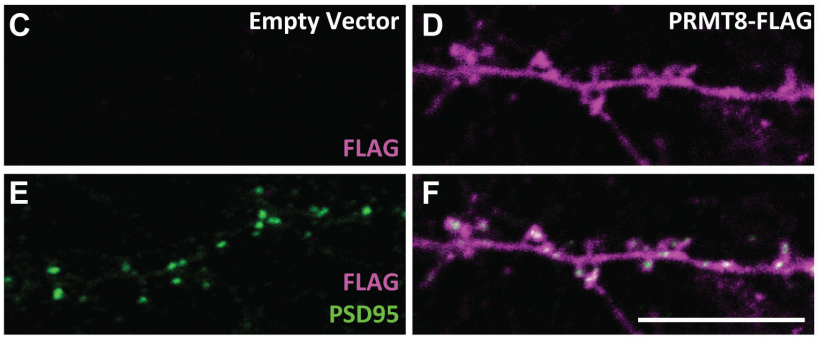

Figure 2

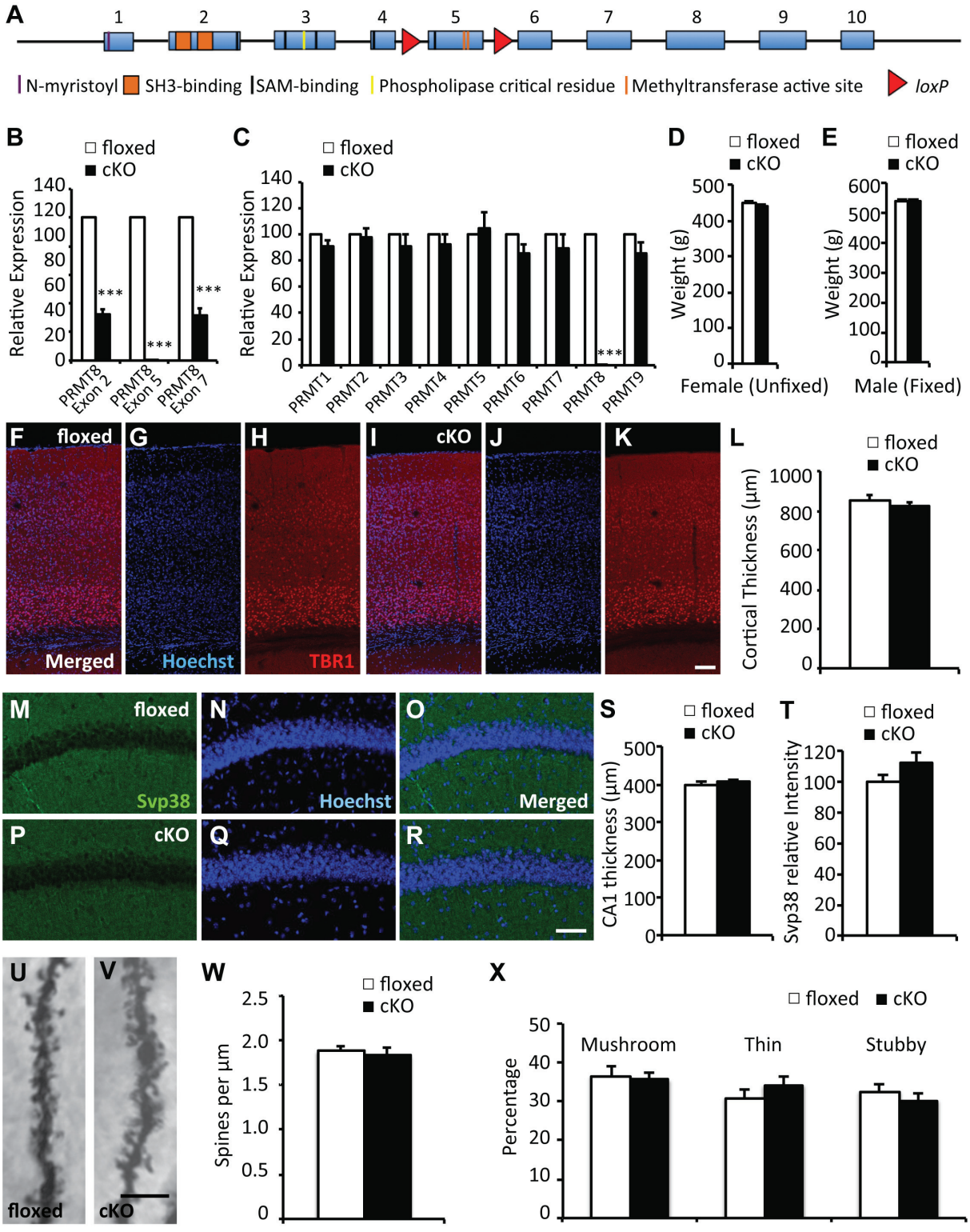

Figure 3

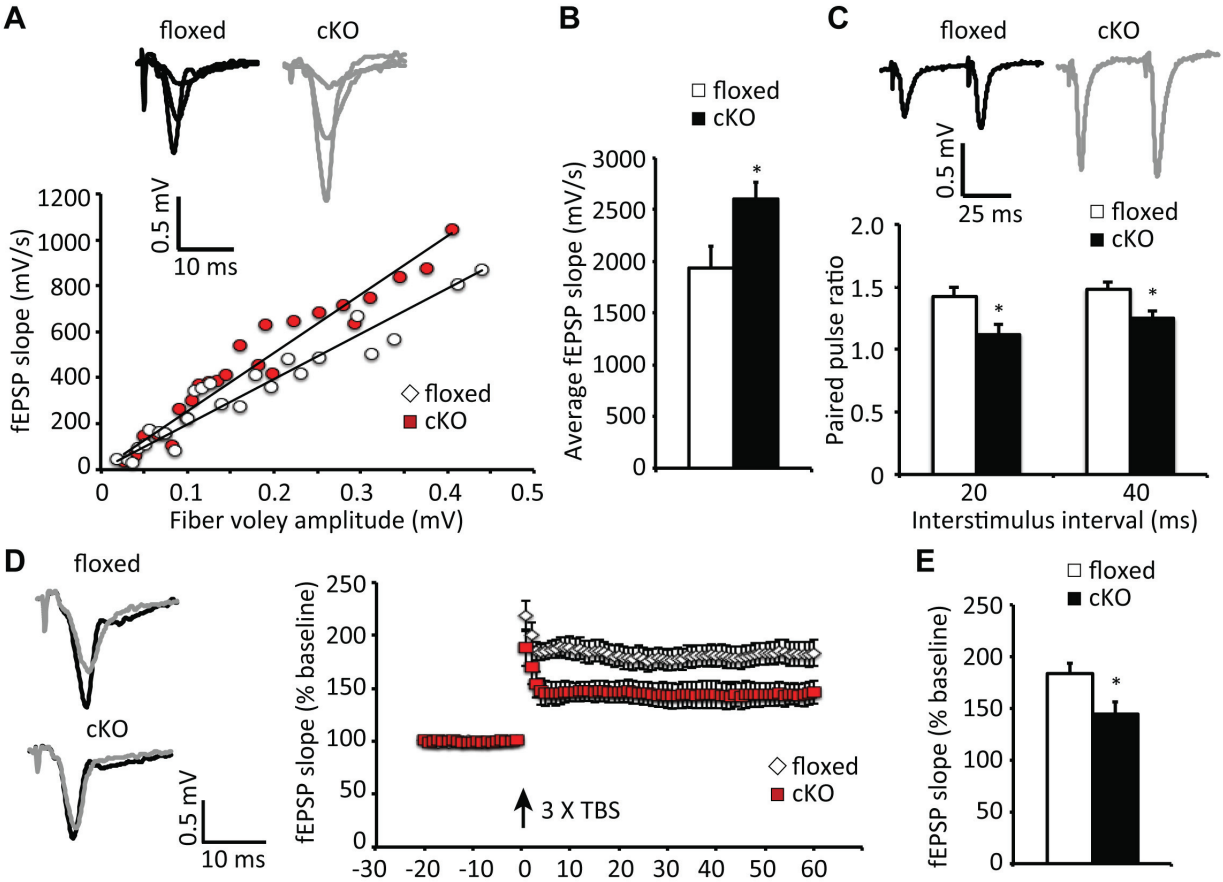

Figure 4

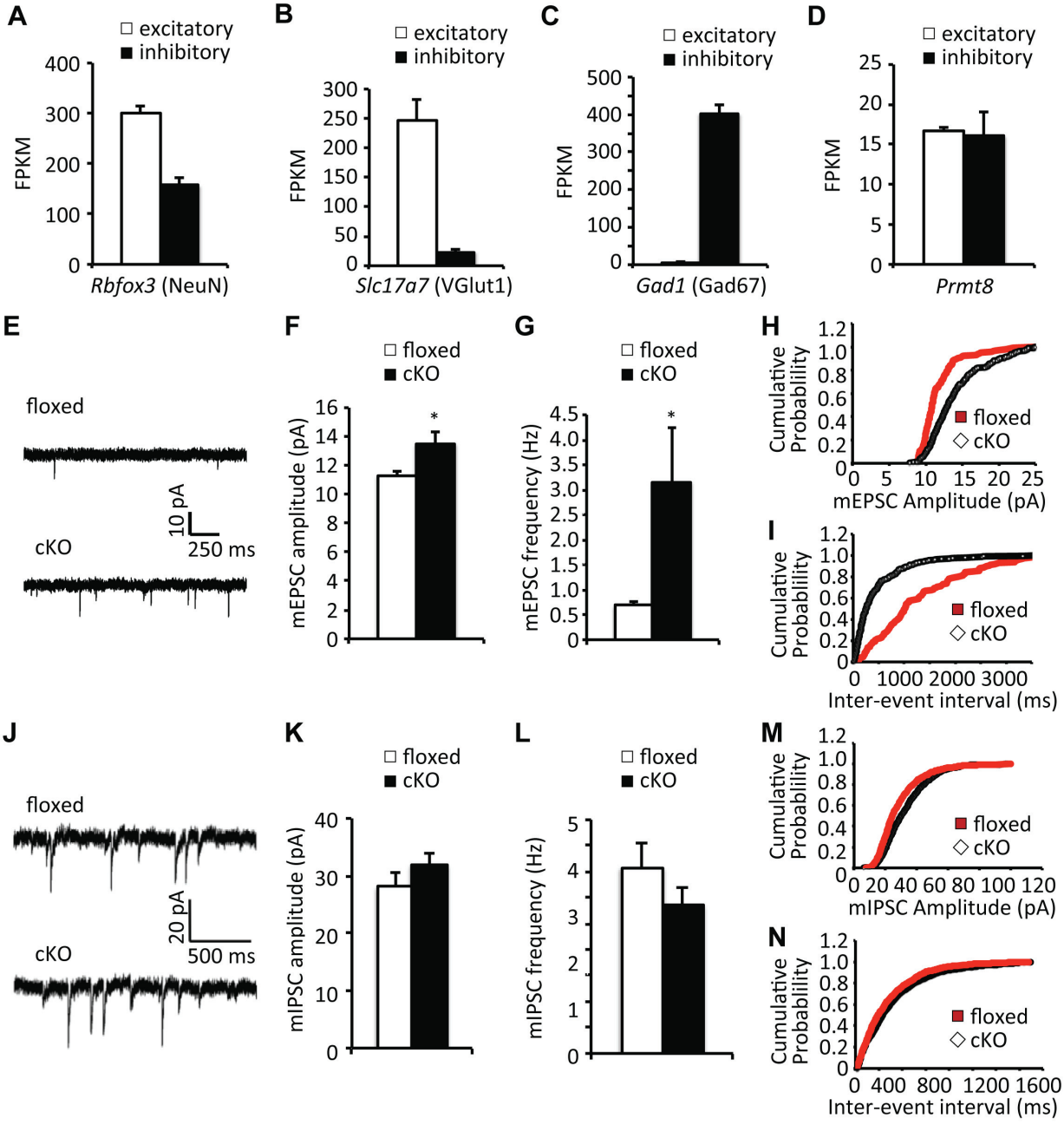

Figure 5

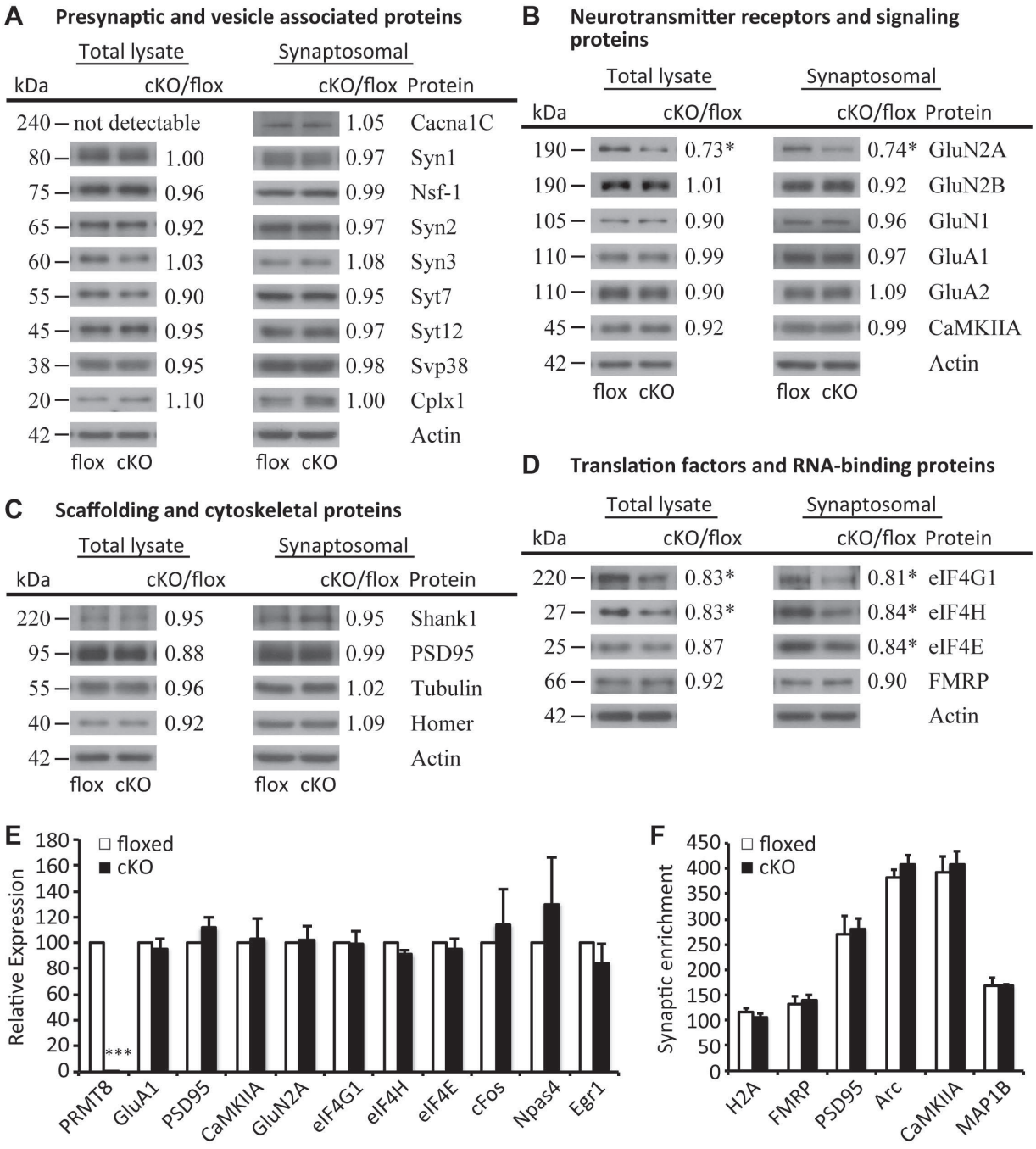

Figure 6

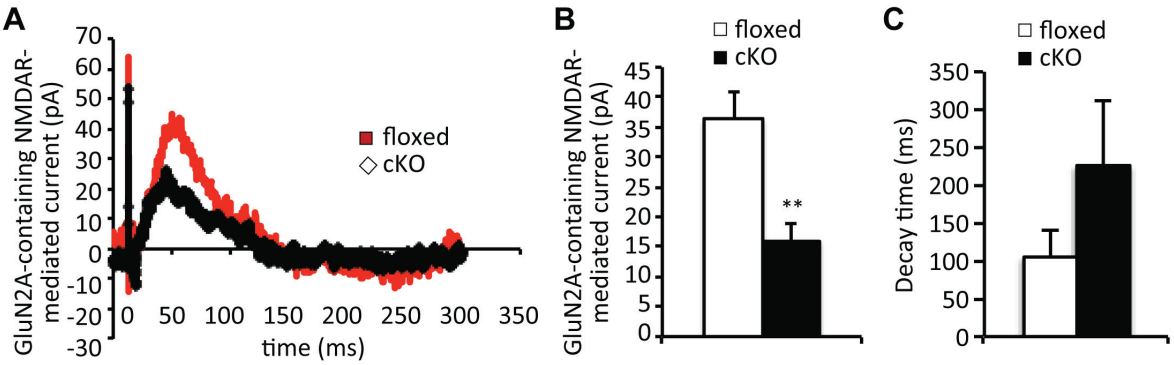

Figure 7